Energetics of Mesoporous Silica: Investigation into Pore Size and Symmetry

Olga Trofymluk,[†] Andrey A. Levchenko,[†] Sarah H. Tolbert,[‡] and Alexandra Navrotsky*,[†]

Thermochemistry Facility and NEAT ORU, University of California at Davis, Davis, California 95616, and Department of Chemistry and Biochemistry, University of California at Los Angeles, Los Angeles, California 90095

Received February 17, 2005. Revised Manuscript Received May 4, 2005

Two families of calcined highly ordered mesoporous silicas, designed as M41S (MCM-41 and MCM-48) and SBA-*n* (SBA-15 and SBA-16), are investigated in a wide range of pore sizes from 2.1 to 26.4 nm by high-temperature oxide melt solution calorimetry using lead borate solvent at 974 K. These data are consistent with and extend our earlier studies of zeolite microporous and of mesoporous silicas. The formation enthalpies observed are 19.0−31.4 kJ/mol less exothermic than that of quartz and correlate linearly with pore size for a given structure type. Small- and wide-angle X-ray scattering, nitrogen adsorption (BET), thermogravimetric analysis, and ^{29}Si NMR are employed to give insight into structure and symmetry. The enthalpy differences among samples are discussed in terms of symmetry and structural (point and ring) defects in the materials.

Introduction

Much progress in the synthesis of microporous and mesoporous molecular sieves with a great variety of framework structures and pore sizes has been made over the past decade. Emerging and promising applications of these materials now include not only catalysis, separation, and ion exchange[1−5] but also more unusual uses, such as contrast agents for diagnostic magnetic resonance imaging;[5,6] hosts for laser dyes;[7−9] and templates for metal nanowires,[10−12] semiconductor nanowires,[13,14] carbon nanotubes, and polymer−carbon composites.[15] The choice of the structure-directing agent (SDA) in combination with inorganic framework and postsynthesis treatment are key factors in gaining control over the materials properties and structure. The nature, concentration, and strength of active sites, as well as the symmetry and size of the channels, are among important characteristics that can be tuned in synthesis and post-treatment. Various experimental techniques including in situ synchrotron X-ray and neutron scattering,[16−19] calorimetry,[20−23] TEM,[24] NMR, and FTIR,[16,25−34] and theoretical approaches

* Corresponding author. Phone: 530-752-3292. Fax: 530-752-9307. E-mail address: anavrotsky@ucdavis.edu.

[†] University of California at Davis.

[‡] University of California at Los Angeles.

(1) Corma, A. *Chem. Rev.* **1997**, *97* (6), 2373.
(2) Estermann, M.; Mccusker, L. B.; Baerlocher, C.; Merrouche, A.; Kessler, H. *Nature* **1991**, *352* (6333), 320.
(3) Han, Y. J.; Stucky, G. D.; Butler, A. *J. Am. Chem. Soc.* **1999**, *121* (42), 9897.
(4) Wang, S.; Choi, D. G.; Yang, S. M. *Adv. Mater.* **2002**, *14* (18), 1311.
(5) Davis, M. E. *Nature* **2002**, *417* (6891), 813.
(6) Lauffer, R. B. *Chem. Rev.* **1987**, *87* (5), 901.
(7) Ihlein, G.; Junges, B.; Junges, U.; Laeri, F.; Schuth, F.; Vietze, U. *Appl Organomet. Chem.* **1998**, *12* (5), 305.
(8) Vietze, U.; Krauss, O.; Laeri, F.; Ihlein, G.; Schuth, F.; Limburg, B.; Abraham, M. *Phys. Rev. Lett.* **1998**, *81* (21), 4628.
(9) Ihlein, G.; Schuth, F.; Krauss, O.; Vietze, U.; Laeri, F. *Adv. Mater.* **1998**, *10* (14), 1117.
(10) Han, Y. J.; Kim, J. M.; Stucky, G. D. *Chem. Mater.* **2000**, *12* (8), 2068.
(11) Ryoo, R.; Ko, C. H.; Kruk, M.; Antochshuk, V.; Jaroniec, M. *J. Phys. Chem. B* **2000**, *104* (48), 11465.
(12) Huang, M. H.; Choudrey, A.; Yang, P. D. *Chem. Commun.* **2000** (12), 1063.
(13) Tanev, P. T.; Pinnavaia, T. J. *Chem. Mater.* **1996**, *8*,. (8), 2068.
(14) Bruinsma, P. J.; Kim, A. Y.; Liu, J.; Baskaran, S. *Chem. Mater.* **1997**, *9* (11), 2507.
(15) Parmentier, J.; Saadhallah, S.; Reda, M.; Gibot, P.; Roux, M.; Vidal, L.; Vix-Guterl, C.; Patarin, J. *J. Phys. Chem. Solids* **2004**, *65* (2−3), 139.
(16) Flodstrom, K.; Wennerstrom, H.; Alfredsson, V. *Langmuir* **2004**, *20* (3), 680.
(17) Zholobenko, V. L.; Khodakov, A. Y.; Durand, D. *Microporous Mesoporous Mater.* **2003**, *66* (2−3), 297.
(18) Edler, K. J.; Reynolds, P. A.; White, J. W. *J. Phys. Chem. B* **1998**, *102* (19), 3676.
(19) Ehrburger-Dolle, F.; Morfin, I.; Geissler, E.; Bley, F.; Livet, F.; Vix-Guterl, C.; Saadallah, S.; Parmentier, J.; Reda, M.; Patarin, J.; Iliescu, M.; Werckmann, J. *Langmuir* **2003**, *19* (10), 4303.
(20) Petrovic, I.; Navrotsky, A.; Davis, M. E.; Zones, S. I. *Chem. Mater.* **1993**, *5* (12), 1805.
(21) Navrotsky, A.; Petrovic, I.; Hu, Y.; Chen, C. Y.; Davis, M. E. *J. Non-Cryst. Solids* **1995**, *193*, 474.
(22) Navrotsky, A.; Petrovic, I.; Hu, Y. T.; Chen, C. Y.; Davis, M. E. *Microporous Mater.* **1995**, *4* (1), 95.
(23) Petrovic, I.; Navrotsky, A.; Chen, C. Y.; Davis, M. E. *Stud. Surf. Sci. Catal.* **1994**, *84*, 677.
(24) Janssen, A. H.; Van Der Voort, P.; Koster, A. J.; de Jong, K. P. *Chem. Commun.* **2002** (15), 1632.
(25) Haddad, E.; Nossov, A.; Guenneau, F.; Gedeon, A. *Cr. Chim.* **2004**, *7* (3−4), 305.
(26) Shi, L.; Zou, Y.; He, H. Y. *Chem. Lett.* **2001** (11), 1164.
(27) Das, N.; Eckert, H.; Hu, H. C.; Wachs, I. E.; Walzer, J. F.; Feher, F. J. *J. Phys. Chem.-Us* **1993**, *97* (31), 8240.
(28) Luan, Z. H.; Meloni, P. A.; Czernuszewicz, R. S.; Kevan, L. *J. Phys. Chem. B* **1997**, *101* (44), 9046.
(29) Chao, K. J.; Wu, C. N.; Chang, A. S.; Hu, S. F. *Microporous Mesoporous Mater.* **1999**, *27* (2−3), 287.
(30) Chao, K. J.; Wu, C. N.; Chang, H.; Lee, L. J.; Hu, S. F. *J. Phys. Chem. B* **1997**, *101* (33), 6341.
(31) Wu, C. N.; Tsai, T. S.; Liao, C. N.; Chao, K. J. *Microporous Mater.* **1996**, *7* (4), 173.
(32) Zhao, X. S.; Lu, G. Q.; Whittaker, A. K.; Millar, G. J.; Zhu, H. Y. *J. Phys. Chem. B* **1997**, *101* (33), 6525.
(33) Luan, Z. H.; Maes, E. M.; van der Heide, P. A. W.; Zhao, D. Y.; Czernuszewicz, R. S.; Kevan, L. *Chem. Mater.* **1999**, *11* (12), 3680.
(34) Morey, M. S.; O'Brien, S.; Schwarz, S.; Stucky, G. D. *Chem. Mater.* **2000**, *12* (4), 898.

10.1021/cm050366g CCC: $30.25
Published on Web 06/11/2005

such as ab initio and Monte Carlo calculations[35−37] successfully have been employed to address issues pertaining to the formation of mesoporous materials and the driving forces for framework assembly.

In addition to developing a clearer understanding of the formation mechanisms of mesoporous frameworks, it is highly desirable to construct thermally and hydrothermally stable porous materials with large pores.[38,39] Although zeolites are well-studied microporous materials with highly organized crystalline structure, their channel dimensions are limited to <2 nm.[5] A major challenge is to overcome this limitation and design ordered frameworks with large pores. Larger pores from 2 to 30 nm are now easy to obtain in mesoporous silica molecular sieves with amorphous walls.[40,41]

Knowledge about energetics of different zeolites and mesoporous materials provides a fundamental basis for understanding driving forces in synthesis, diversity among structures, as well as formation mechanisms and interactions during framework assembly. It is intuitively obvious that less stable frameworks are more difficult to synthesize and retain.[35] However, previous calorimetric data[20−22] on high-silica zeolites and mesoporous silica (MCM-41) suggest little energetic limitation to structures that can form. Indeed, it has been reported that the formation enthalpy of mesoporous MCM-41 silicas levels off at about 14−15 kJ/mol relative to quartz for pores of 2−4 nm diameters.[20] Moreover, such moderate metastability implies that selection among configurations and/or structures, which would have similar energies, is governed by kinetic factors, rather than by thermodynamics. These small energetic limitations allow a diversity of synthesized frameworks.

The calorimetric study of MCM-41[21,22] was limited by pore sizes (2−4 nm) and quality of mesoporous materials available a decade ago. The mesoporous materials were not as pure and well-characterized as can now be made. Recent calorimetric results by Piccione et al.[42] on zeolites (with a larger number of better characterized samples) confirmed findings by Petrovic et al.[20] that the range of energies is quite narrow (6.8−14.4 kJ/mol above quartz) and firmly established a correlation of formation enthalpy with framework density and molar volume. These results are consistent with earlier computer simulations by Kramer et al.[43] and de vos Burchart et al.[44] suggesting less stable structures should be observed in less dense frameworks. Later Moloy et al.[43] performed molecular modeling and found that the internal surface area correlates well with the formation enthalpy of anhydrous silica zeolites. Also they found that the internal surface enthalpy of silica zeolites is quite low (0.10 J/m^2) and similar to the surface energy of amorphous silica. All these findings might impose some energetic constraints to synthesis of zeolites with extra large pores. Recent theoretical studies by Zwijnenberg et al.[35,36] addressed this issue in terms of face-size distribution as a direct measure of zeolite synthesis viability.

To arrive at more definite conclusions regarding effects of various structural parameters on energetics, experimental thermodynamic data are required for pure-silica mesoporous materials over a wider range of pore sizes and structures than available to the Navrotsky et al. study.[21] In the past few years the use of nonionic triblock and star diblock copolymers, as well as oligomeric surfactants, has enabled synthesis of highly ordered, thermally, and hydrothermaly stable mesoporous silicas with pore sizes up to 30 nm.[40,41,45] In addition, a family of cubic phases MCM-48 has received much attention due to its intrinsic three-dimensional connected channel structure, which is very promising for catalyst applications.[1] Calorimetric data for the cubic phase are not yet available. Therefore, new insights into energetics of mesoporous molecular sieves will permit us not only to establish the range of relative thermodynamic stability but also to predict the energy landscape for desirable but yet unmade porous materials.

In this report, the formation enthalpy ($\Delta H_{\mathrm{form}}^{298}$) relative to quartz of pure-SiO_2 molecular sieves with hexagonal (MCM-41 and SBA-15) and cubic (MCM-48 and SBA-16) structures in a wide range of pore sizes from 2.5 to 26.4 nm for hexagonal and 2.1−5.4 nm for cubic is examined by high-temperature oxide melt calorimetry using lead borate as solvent at 974 K. It has to be stressed here that, for the first time, the formation enthalpy of cubic mesoporous silica molecular sieves is reported. In addition, the surface energy is estimated where possible.

Experimental Section

Materials. MCM-41_1 silica was synthesized according to the method of Gallis et al.[46] using *n*-hexadecyltrimethylammonium bromide (CTAB, Alfa Aesar) as a structure-directing agent. NaOH (2 M, 5.0 g) was added to 39.2/0.8 g of aqueous surfactant solution. After heating to 303−313 K to dissolve the surfactant, the silicate source, 3.85 g of tetraethoxysilane (TEOS, Aldrich), was added to the solution under constant stirring. After 3 h of stirring the precipitated product was filtered and washed with deionized (DI) water. MCM-41_2 was prepared using the same composition as reported by Khushalani et al.[47] The following is a typical preparation procedure: 3.6 g of Cab-o-Sil silica is suspended in 6 g of water under vigorous stirring and then 6.16 g of 25 wt % tetramethylammonium hydroxide (TMAOH) was added. Separately, 3.65 g of CTAB was dissolved in 6.56 g of water, and subsequently, 1.17

(35) Zwijnenburg, M. A.; Bromley, S. T.; Foster, M. D.; Bell, R. G.; Delgado-Friedrichs, O.; Jansen, J. C.; Maschmeyer, T. *Chem. Mater.* **2004**, *16* (20), 3809.
(36) Zwijnenburg, M. A.; Bromley, S. T.; Jansen, J. C.; Maschmeyer, T. *Chem. Mater.* **2004**, *16* (1), 12.
(37) Kuchta, B.; Llewellyn, P.; Denoyel, R.; Firlej, L. *Colloid Surf. A* **2004**, *241* (1−3), 137.
(38) Mokaya, R. *J. Phys. Chem. B* **1999**, *103* (46), 10204.
(39) Cassiers, K.; Linssen, T.; Mathieu, M.; Benjelloun, M.; Schrijnemakers, K.; Van Der Voort, P.; Cool, P.; Vansant, E. F. *Chem. Mater.* **2002**, *14* (5), 2317.
(40) Zhao, D. Y.; Feng, J. L.; Huo, Q. S.; Melosh, N.; Fredrickson, G. H.; Chmelka, B. F.; Stucky, G. D. *Science* **1998**, *279* (5350), 548.
(41) Zhao, D. Y.; Huo, Q. S.; Feng, J. L.; Chmelka, B. F.; Stucky, G. D. *J. Am. Chem. Soc.* **1998**, *120* (24), 6024.
(42) Piccione, P. M.; Laberty, C.; Yang, S. Y.; Camblor, M. A.; Navrotsky, A.; Davis, M. E. *J. Phys. Chem. B* **2000**, *104* (43), 10001.
(43) Kramer, G. J.; Deman, A. J. M.; Vansanten, R. A. *J. Am. Chem. Soc.* **1991**, *113* (17), 6435.
(44) Burchart, E. D.; Verheij, V. A.; Vanbekkum, H.; Vandegraaf, B. *Zeolites* **1992**, *12* (2), 183.
(45) Zhao, D. Y.; Yang, P. D.; Huo, Q. S.; Chmelka, B. F.; Stucky, G. D. *Curr. Opin. Solid State Mater.* **1998**, *3* (1), 111.
(46) Gallis, K. W.; Landry, C. C. *Chem Mater* **1997**, *9* (10), 2035.
(47) Khushalani, D.; Kuperman, A.; Ozin, G. A.; Tanaka, K.; Garces, J.; Olken, M. M.; Coombs, N. *Adv. Mater.* **1995**, *7* (10), 842.

g of 30 wt % NH_4OH was introduced. The mixtures containing the silica and CTAB were stirred together for 30 min, transferred into a Teflon-lined autoclave, and treated under autogenous pressure without stirring at 343 K for 72 h. Then the sample was filtered and washed with DI water.

MCM-48 silica of different pore sizes was synthesized as reported by Gallis et al.[46] using a bulk-phase transformation procedure. After the silicate mixture was stirred for 20 min (MCM-48_1) and 2 h (MCM-48_2), the reaction mixture was transferred to a Teflon-lined steel Parr autoclave and, depending on the desired pore size, heated at 373 K for 6 days (MCM-48_1) and 423 K for 4 h (MCM-48_2). After the autoclaves were cooled, the precipitated product was filtered and washed with DI water.

Mesoporous silica SBA-15 phases of different pore diameters were synthesized as reported by Zhao et al.,[40,41] using commercially available BASF Pluronic P123 ($M_w = 5.8$K) as a SDA. In a typical preparation procedure, 4 g of Pluronic P123 was dissolved with stirring in 30 g of water and 120 g of 2 M HCl solution at 308 K. Then 8.5 g of TEOS was added into that solution under stirring. The mixture was maintained at 308 K for 10−12 h and then at 333 K for 48 h and then aged at higher temperature between 373 and 393 K for 24 or 48 h under static conditions in a Teflon-lined autoclave to generate materials with uniform pore diameter from 4 to 10 nm. The solid product was recovered and washed with DI water. The pore size of SBA-15 has been extended to 25 nm by the addition of cosolvent organic molecules, such as 1,3,5-trimethylbenzene (TMB).

SBA-16 silicas were synthesized under acidic condition at room temperature, using Puronic F127 ($M_w = 12.6$K) as a SDA.[40,41] In a typical preparation procedure, 1.5 g of Pluronic F127 was dissolved under starring in 30 g of water and 120 g of 2 M HCl solution at 298 K. Then 8.5 g of TEOS was added into that solution with stirring. After reacting at room temperature for 20 h, ordered SBA-16 was produced by aging the solid precipitate at temperatures between 368 and 378 K for 48 h under static conditions in a Teflon-lined autoclave. The solid product was recovered and washed with DI water.

Calcination for all materials was carried out in a Thermolyne Type 21100 tube furnace with West 2050 microprocessor-based programmer controller by slow heating at 1 K/min from room temperature to 773 K and holding at this temperature for 6 h under N_2 and another 6 h under O_2. After calcination the furnace tube was sealed under Ar and transferred into an Ar-filled glovebox, where all the samples were stored to prevent atmospheric moisture adsorption. For calorimetry, samples were pressed into 5-mg pellets inside the glovebox; each pellet was placed into a vial with a cap for transport to the calorimeter.

Characterization. Powder XRD experiments were carried out on an Inel X-ray diffractometer (XRG 3000) operated at 30 kV and 30 mA using Cu Kα radiation with an Ni-filter. Data were collected in the 2θ range of 1.5°−10°. Small-angle XRD patterns at 2θ from 0.1° to 3.0° were recorded on a Bruker NanoSTAR SAXS apparatus with a two-dimensional detector using Cu Kα radiation.

The adsorption/desorption isotherms of nitrogen at 77 K were measured using a Micromeritics ASAP 2020 instrument. Each sample was outgassed at 473 K until a stable static vacuum of 3×10^{-3} Torr was reached. The specific surface area of the materials (also designated here as total surface area) was calculated according to the Brunauer−Emmett−Teller (BET) equation[48,49] using specific range from 0.05 to 0.3. Mesopore size distributions were calculated from adsorption isotherm using the Barrett−Joyner−Halenda (BJH) method.[50] To evaluate the wall thickness, a reliable value of pore size is required. It is widely accepted that the maximum of the BJH method underestimates the size of pores.[51,52] Therefore, the more precise geometric relation developed by Kruk et al.[53] for hexagonal mesostructure was used to calculate the primary mesopore diameter and wall thickness of MCM-41 and SBA-15. The volume of primary (ordered) mesopores (V_p) and external surface area were assessed according to the α_s-method by Kruk et al.[53] The external surface area was calculated in the α_s range from 2 to 2.5. V_p was measured by extrapolating the linear part after the capillary condensation step to $\alpha_s = 0$. The primary mesopore diameter was obtained from the maximum of the Kruk−Jaroniec−Sayari (KJS) pore size distribution, which is based on a corrected Kelvin equation and yields more accurate value than the BJH maximum for MCM-48 materials.[54,55] Due to complex curvature of the cubic MCM-48 and SBA-16 channels, the simple geometric models available to the BET evaluation cannot be applied. However, the wall thickness of MCM-48 and SBA-16 was calculated from adsorption and SAXS data using a theory developed recently by Ravikovitch and Neimark.[56]

Solid-state ^{29}Si NMR spectra for all samples were collected on a CMX Infinity 400 spectrometer at a frequency of 79.489 MHz based on a 9.4 T magnet. The samples were packed into a 7 mm ZrO_2 rotor and spun at 5 kHz. Single pulse excitation ^{29}Si NMR spectra were recorded using a ^{29}Si 45° pulse length of 4 μs, a recycle delay of 60 s, and 1000 scans. The ^{29}Si CP MAS NMR spectra were acquired with 5 ms contact time at ramped mixing level, 5 s recycle delay, and 1000 scans. The ^{29}Si NMR chemical shift was externally referenced to tetramethylsilane (TMS). The spectra were analyzed by fitting observed data into Gaussian lines.

Thermogravimetric analyses (TGA) were performed on 15−20 mg samples using a Netzsch STA 449 system to measure the mass fraction of water present in the samples introduced into the calorimeter. The heating rate was 10 K/min to 1473 K, and dry Ar was used as a carrier gas to avoid sample rehydratation. Buoyancy corrections were performed for all runs by allowing the sample to cool to room temperature and heating it back to 1473 K. Gases evolved during thermal analysis were analyzed by a Bruker EQUINOX 55 FTIR spectrometer, which is directly coupled with the TG/DSC by a heated transfer line kept at 423 K. FTIR spectra of evolved gases were collected from 400 to 4000 cm^{-1} at a resolution of 4 cm^{-1}. A baseline correction was made before each run.

High-Temperature Calorimetry. Drop solution calorimetry was employed to obtain the heats of solution of pure silica materials. In each experiment, the sample pellet was dropped from a vial, sealed at room temperature under argon, into the molten $2PbO \cdot B_2O_3$ solvent in the calorimeter at 973 K. A quartz sample (Fluka, 99.5%) was used in addition to mesoporous silica materials so that the transition enthalpy for the reaction

$$\text{quartz (298 K)} \rightarrow \text{mesoporous silica (298 K)} \quad \Delta H_{\text{form}}^{298} \quad (1)$$

(48) Brunauer, S.; Emmett, P. H.; Teller, E. *J. Am. Chem. Sci.* **1938**, *60*, 308.
(49) Sing, K. S. W.; Everett, D. H.; Haul, R. A. W.; Moscou, L.; Pierotti, R. A.; Rouquerol, J.; Siemieniewska, T. *Pure Appl. Chem.* **1985**, *57* (4), 603.
(50) Barrett, E. P.; Joyner, L. G.; Halenda, P. P. *J. Am. Chem. Soc.* **1951**, *73*, 373.
(51) Galarneau, A.; Desplantier, D.; Dutartre, R.; Di Renzo, F. *Microporous Mesoporous Mater.* **1999**, *27* (2−3), 297.
(52) Zhu, H. Y.; Zhao, X. S.; Lu, G. Q.; Do, D. D. *Langmuir* **1996**, *12* (26), 6513.
(53) Kruk, M.; Jaroniec, M.; Sayari, A. *Chem. Mater.* **1999**, *11* (2), 492.
(54) Kruk, M.; Jaroniec, M.; Sayari, A. *Langmuir* **1997**, *13* (23), 6267.
(55) Kruk, M.; Jaroniec, M.; Ryoo, R.; Joo, S. H. *Chem. Mater.* **2000**, *12* (5), 1414.
(56) Ravikovitch, P. I.; Neimark, A. V. *Langmuir* **2000**, *16* (6), 2419.

Table 1. Physicochemical Properties of Mesoporous Silica

sample	surfactant	d_{100} (nm)	a (nm)	BET surface area (m^2/g)	pore size (nm)	V_p (cm^3/g)	V_{mi} (cm^3/g)	S_{ex} (m^2/g)	molar volume (cm^3/mol)	wall thickness (nm)
MCM-41_1	CTAB	3.2	3.7	1263	2.8	0.62	0.008	74	71.59	1.4
MCM-41_2	CTAB	4.9	5.7	1258	4.4	0.67	0.01	68	72.79	1.5
SBA-15_1	P123	6.4	7.4	617	5.6	1.06	0.07	84	110.04	2.8
SBA-15_2	P123	7.1	8.2	627	6.5	0.54	0.08	81	102.83	2.7
SBA-15_3	P123	7.6	8.8	826	7.1	1.00	0.12	101	66.78	2.7
SBA-15_4	P123	8.2	9.5	766	8.2	1.10	0.09	178	100.43	2.8
SBA-15_5	P123	8.5	9.8	725	8.5	1.06	0.10	174	93.82	2.3
SBA-15_6	P123	10.0	11.6	850	10.1	1.03	0.10	192	104.63	3.5
SBA-15_7	P123	10.6	12.2	725	10.7	1.17	0.10	138	96.22	3.1
SBA-15_8	P123/TMB	12.1	14.0	770	12.2	1.61	0.12	152	131.07	3.3
SBA-15_9	P123/TMB	15.2	17.6	890	15.2	1.22	0.11	164	107.64	4.5
SBA-15_10	P123/TMB	19.0	21.9	860	19.0	1.12	0.14	179	86.61	5.2
SBA-15_11	P123/TMB	21.6	24.9	728	21.8	1.09	0.14	127	87.81	6.1
SBA-15_12	P123/TMB	23.0	26.6	858	23.7	1.84	0.14	195	145.49	5.7
SBA-15_13	P123/TMB	25.5	29.5	806	26.4	2.21	0.14	172	167.12	5.9
MCM-48_1	CTAB	68	68	1328	2.1	0.63	0.01	147	72.19	1.3
MCM-48_2	CTAB	78	78	1245	2.6	0.69	0.02	123	75.79	1.3
SBA-16_1	F127	99	99	826	4.8	0.34	0.03	107	58.97	1.1
SBA-16_2	F127	108	108	827	5.4	0.46	0.03	147	61.97	1.0

could be obtained. This reaction is endothermic (positive transition enthalpy); quartz is more stable than mesoporous silica. All thermochemical measurements were performed using a Tian-Calvet twin microcalorimeter that has been described in detail elsewhere,[57] operating under flowing Ar to assist the removal of any water vapor. The calibration factors for the calorimeter ($J/\mu V$) were obtained by dropping 5- and 15-mg pellets of alumina (Aldrich, 99.99%) stabilized in the corundum phase by heating overnight at 1773 K. The overall methodology is now standard and has been reported previously.[20,42,57]

Results and Discussion

Structure and Properties of Mesoporous Silicas. Diffraction patterns of calcined MCM-41 and SBA-15 materials show four or five well-resolved peaks with indices (10), (11), (20), (21), and (30), and in all cases, the pattern conforms to a two-dimensional hexagonal lattice (*p*6*mm* space group). The lattice parameter *a* for the two calcined MCM-41 samples studied is 3.7 and 5.7 nm, respectively. A 3.6% contraction was observed for MCM-41 after calcination. The cell parameter for calcined SBA-15 samples ranges from 7.4 to 12.2 nm (without TMB as the organic pore swelling agent) and from 14.0 to 29.5 nm (with TMB). Calcinations of SBA-15 without TMB led to a 5−6% contraction. Values of the *d* spacing between the (10) planes of the arrays of pores in the silica materials and lattice parameter *a* are given in Table 1. The XRD patterns of SBA-16 show reflections corresponding to a cubic structure (*Im*3*m* space group) with indices (110), (200), (211), (220), (310), (222), and (321). Reflections in diffractograms for MCM-48 index to the *Ia*3*d* cubic lattice (the *a* parameter is shown in Table 1). All the above results are in good agreement with previously reported data.[41,58,59]

Nitrogen adsorption isotherms for the calcined MCM-41, MCM-48, and SBA-16 silicas exhibit a steep pore condensation step without adsorption hysteresis or a narrow hysteresis loop as reported in previous studies.[39,60−62] The sharpness of the capillary condensation steps indicates uniformity of pore channels and their narrow pore size distribution. The sorption isotherms for SBA-15 materials exhibit a nearly ideal H1 type hysteresis loop, with almost vertical steps on the ascending and descending curves, as expected for pore condensation in open cylindrical pores at a temperature well below the pore critical temperature. At pressures above the pore condensation step, the nitrogen sorption isotherms of most materials show only a weak further increase with pressure, indicative of the high bulk modulus of these materials.

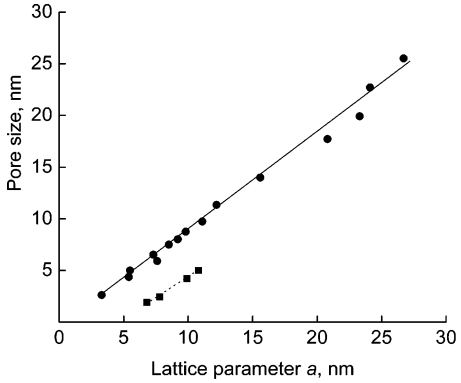

Figure 1. Pore size as a function of lattice parameter *a*: ●, hexagonal MCM-41 and SBA-15; ■, cubic MCM-48 and SBA-16.

It is remarkable that both hexagonal and cubic symmetries exhibit a linear dependence of pore diameter plotted as a function of the unit cell parameter *a* (Figure 1 and Table 1). These results suggest that a more expended lattice is generally required to stabilize and accommodate larger pores. According to the model by Kruc et al.,[63] the lattice size for hexagonal pores is governed by two competitive factors: the lattice expansion of the framework, primarily due to the SDA micelle size increase, and shrinkage during the posttreatment.

(57) Navrotsky, A. *Phys. Chem. Miner.* **1977**, *2* (1−2), 89.
(58) Kresge, C. T.; Leonowicz, M. E.; Roth, W. J.; Vartuli, J. C.; Beck, J. S. *Nature* **1992**, *359* (6397), 710.
(59) Beck, J. S.; Vartuli, J. C.; Roth, W. J.; Leonowicz, M. E.; Kresge, C. T.; Schmitt, K. D.; Chu, C. T. W.; Olson, D. H.; Sheppard, E. W.; Mccullen, S. B.; Higgins, J. B.; Schlenker, J. L. *J. Am. Chem. Soc.* **1992**, *114* (27), 10834.
(60) Cheng, C. F.; Lin, Y. C.; Cheng, H. H.; Chen, Y. C. *Chem. Phys. Lett.* **2003**, *382* (5−6), 496.
(61) Kruk, M.; Jaroniec, M.; Ryoo, R.; Kim, J. M. *Chem. Mater.* **1999**, *11* (9), 2568.
(62) Kruk, M.; Jaroniec, M.; Ko, C. H.; Ryoo, R. *Chem. Mater.* **2000**, *12* (7), 1961.
(63) Kruk, M.; Jaroniec, M.; Sayari, A. *J. Phys. Chem. B* **1999**, *103* (22), 4590.

Table 2. Results from Thermogravimetric Analysis of Silica Materials

sample	% mass loss TGA (wt)	*h* (mol H_2O/ mol SiO_2)	MW/ mol SiO_2
quartz	0.27	0.009	60.25
MCM-41_1	1.68	0.057	61.11
MCM-41_2	1.65	0.056	61.09
SBA-15_1	1.32	0.045	60.89
SBA-15_2	1.51	0.051	61.01
SBA-15_3	1.18	0.040	60.80
SBA-15_4	1.32	0.045	60.89
SBA-15_5	1.87	0.064	61.23
SBA-15_6	1.74	0.059	61.15
SBA-15_7	1.83	0.062	61.21
SBA-15_8	1.20	0.040	60.81
SBA-15_9	1.36	0.046	60.91
SBA-15_10	1.28	0.043	60.86
SBA-15_11	1.24	0.042	60.84
SBA-15_12	1.09	0.037	60.75
SBA-15_13	0.98	0.033	60.68
MCM-48_1	1.61	0.055	61.07
MCM-48_2	1.17	0.039	60.80
SBA-16_1	0.90	0.030	60.63
SBA-16_2	0.80	0.027	60.57

The former results from complex interactions between SDA, swelling agent, water, and silica source, whereas the latter is accompanied by structural rearrangement and condensation of silica framework. Indeed, the temperature at different states of sample synthesis and time lead to the pore size and lattice changes for our samples in a nontrivial manner.

The TGA results are shown in Table 2, along with the calculated molar mass per mole of SiO_2 and water content. The amounts of water present in dehydrated samples were calculated by taking the difference of the mass losses at the weight loss plateau (>1173 K) and at the dehydration temperature 373 K. The water contents are typically 1−2 wt %. The hydrothermally synthesized mesoporous materials usually have nonzero water contents even after they are calcined at elevated temperature and kept in an Ar-filled glovebox. This water mostly exists in the form of silanol groups on the silica surface, because the amount of physically adsorbed water is minimized after the sample treatment above 773 K (see Experimental Section for details).

^{29}Si MAS NMR spectra collected for the calcined MS samples consist of a wide asymmetric signal that ranges from −90 to −125 ppm and is dominated by a component centered at −110.5 to −112 ppm, assignable to Q^4 species (Figure 2a−c). This observation is in excellent agreement with the literature for amorphous silica (fumed and treated above 1373 K).[64,65] This implies relatively low (typically, less than 15 mol %) concentration of Q^2 and Q^3 defects in calcined MS as compared to those in as-synthesized MS, where these concentrations reach a 40−50% level.[66,67] The Q^2 and Q^3 chemical shifts are confirmed by ^{29}Si CP MAS spectra (Figure 2d) in which the intensities of silicon resonances of Q^2 and Q^3 sites are greatly enhanced relative to those of Q^4. The chemical shifts at −92 and −100 ppm for Q^2 and Q^3 are in good agreement with the literature.[64] A method by Brinker et al.[64,65] was used to deconvolute Q^2, Q^3, and Q^4 peaks in the ^{29}Si CP MAS spectra. In this method, all the spectra require an additional peak at −105 ppm to account for a second Q^4 ($Q^{4'}$ here) resonance with a less negative chemical shift due to strained rings (see discussion below).

The chemical cycles for dehydroxylation during heating of isolated and geminal hydrosils suggest that one water molecule is formed per one geminal hydroxyl and two single hydroxy groups, respectively:

$$2[-\mathrm{Si(OH)}]\ (\mathrm{s, 298\ K}) \rightarrow -\mathrm{Si-O-Si}-\ (\mathrm{soln, 974\ K}) + \mathrm{H_2O\ (g, 974\ K)} \quad \text{for } Q^3 \text{ sites} \quad (2)$$

$$-\mathrm{Si(OH)_2}\ (\mathrm{s, 298\ K}) \rightarrow -\mathrm{Si-O}-\ (\mathrm{soln, 974\ K}) + \mathrm{H_2O\ (g, 974\ K)} \quad \text{for } Q^2 \text{ sites} \quad (3)$$

Therefore, to compare TG results with NMR deconvolution results, the $(Q^2 + Q^3/2)/(Q^2 + Q^3 + Q^4 + Q^{4'})$ ratios are calculated. A quantitative deconvolution into Gaussian line shape gave $(Q^2 + Q^3/2)/(Q^2 + Q^3 + Q^4 + Q^{4'})$ ratios of 0.056 for MCM-41, 0.053 for MCM-48, and 0.04−0.078 for SBA-15. These results indicate that, compared to hexagonal MCM (MCM-41), hexagonal SBA (SBA-15) has a somewhat less condensed, but similarly locally disordered, silica framework. The best deconvolution results, taking into account the $Q^{4'}$, were obtained with a fixed position of the Q^2 and Q^3 defects and fixed peak breadths as suggested by Brinker et al.[64,65] We did not fix the area under these peaks to compare the fitting results with the TG data. In our calculations the position of $Q^{4'}$ was allowed to vary during fitting, whereas the breadths of all the peaks were fixed at about 10 ppm. The MCM-41 spectrum is significantly narrower than other spectra, yielding unrealistic defect site concentrations, so smaller 9 ppm breadths were chosen. Q^2 was excluded from the calculation of defect concentration as statistically unreliable, if the noise level was higher then the Q^2 intensity. According to the Shi et al. study[26] the concentration of geminal silanols for SBA-15 is 1.5%, 10 times less than other silanols; therefore, this assumption should have a marginal effect on the defect concentration calculation.

The small-angle region of SAXS patterns (not shown) obeys the Porod power law as evidenced by the linear dependence of the intensity on q ($q = 4\pi/\lambda \sin(\theta/2)$) in logarithmic coordinates corrected for the background scattering using a carbon black standard. The least-squares fits to SAXS plots in the range 0.01−0.02 nm^{-1} yield an exponent of 3.85 for MCM-41, 3.91 for SBA-15, and 3.90 for MCM-48. These results are in good agreement with previous synchrotron SAXS and neutron data.[68,69]

Enthalpies of Formation, ΔH_{form}^{298}. The enthalpy of formation for the reaction quartz → mesoporous silica at 298 K was calculated by using the enthalpy of drop solution for quartz and the mesoporous silica ($\Delta H_{dropsol}$). The following thermodynamic cycle was used to determine the energetics of the mesoporous silica frameworks, where MS is a

(64) Brinker, C. J.; Kirkpatrick, R. J.; Tallant, D. R.; Bunker, B. C.; Montez, B. *J. Non-Cryst. Solids* **1988**, *99* (2−3), 418.
(65) Brinker, C. J.; Brow, R. K.; Tallant, D. R.; Kirkpatrick, R. J. *J. Non-Cryst. Solids* **1990**, *120* (1−3), 26.

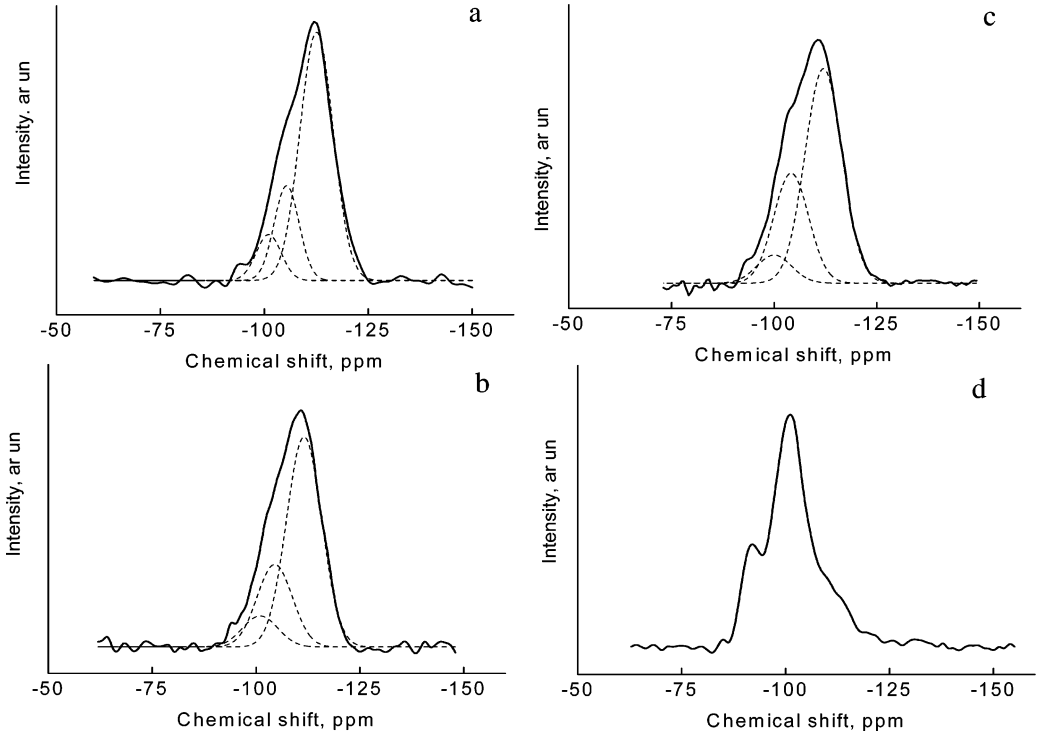

Figure 2. Typical MAS and CP MAS ^{29}Si NMR spectra: (a) ^{29}Si MAS NMR of MCM-41, (b) ^{29}Si MAS NMR of MCM-48, (c) ^{29}Si MAS NMR of SBA-15, and (d) ^{29}Si CP MAS NMR of SBA-15.

designation of any mesoporous silica framework and h is the number of moles of water present per mole of SiO_2:

$$SiO_2\,(\text{soln, 974 K}) + hH_2O\,(\text{g, 974 K}) \rightarrow MS{\cdot}hH_2O\,(\text{s, 298 K}) \quad (4)$$

$$H_2O\,(\text{l, 298 K}) \rightarrow H_2O\,(\text{g, 974 K}) \quad (5)$$

$$SiO_2\,(\alpha\text{-quartz, 298 K}) \rightarrow SiO_2\,(\text{soln, 974 K}) \quad (6)$$

By addition of these equations, $\Delta H_{\text{trans}}^{298}$ for the formation of MS from α-quartz is obtained

$$SiO_2\,(\alpha\text{-quartz, 298 K}) + hH_2O\,(\text{l, 298 K}) \rightarrow MS{\cdot}hH_2O\,(\text{s, 298 K}) \quad (7)$$

where $\Delta H_4 = \Delta H_1 + h\Delta H_2 + \Delta H_3 = \Delta H_{\text{form}}^{298}$.

The enthalpies ΔH_1 and ΔH_3 are the experimentally measured heats of drop solution for the mesoporous materials and quartz, respectively. ΔH_2 obtained from FactSage 5.2 software represents the heat required to completely vaporize and heat the residual amount of water in the dehydrated mesoporous materials from 298 K to the calorimeter operating temperature of 974 K. This correction assumes that the residual H_2O present is energetically the same as liquid water and there is no energetic contribution due to the water−silica surface interaction. This assumption of a zero hydration enthalpy for calorimetric experiments has been a subject for debate in the literature.[42,70] Piccione et al.[42] estimated the transition enthalpies for pure silica zeolites with a correction of 10 kJ/mol on water content due to the hydration enthalpy. The highest water content of 1.87 wt % observed for SBA15−5 yields the largest estimated discrepancy of 0.66 kJ/mol between values that ignore and take into account the possible hydration enthalpy in the transition enthalpy. This discrepancy is within the typical experimental error and does not change the picture of the energy landscape.

The measured enthalpies of drop solution $\Delta H_{\text{dropsol}}$ for all the silica mesoporous molecular sieves relative to quartz are presented in Table 3; the corresponding pore sizes are listed as well. Experimental value of $\Delta H_{\text{dropsol}}$ for quartz are within experimental error of the previous value[42,71] of 39.8 ± 0.3 kJ/mol.

The Overall Picture of the Energy Landscape. To present the experimental data on energetics of mesoporous silica, the transition enthalpies are plotted as a function of pore size for all the samples studied. As shown in Figure 3 and Table 3, the transition enthalpy changes from 19.0 to 31.4 kJ/mol and correlates approximately linearly with the pore size. It is expected that the MS with larger pores are obtained at the cost of higher instability. However, an increase in pore size of more than a factor of 10 results in an only 12.4 kJ/mol less stable framework (Table 3). This value is approximately four times the thermal energy available in the typical synthesis around 373 K. This means that proper synthesis pathways can overcome such a moderate energy barrier.

(66) Wang, Y. Q.; Yang, C. M.; Zibrowius, B.; Spliethoff, B.; Linden, M.; Schuth, F. *Chem. Mater.* **2003**, *15* (26), 5029.
(67) Wang, L. M.; Fan, H.; Tian, B. Z.; Yang, H. F.; Yu, C. Z.; Tu, B.; Zhao, D. Y. *Microporous Mesoporous Mater.* **2004**, *67* (2−3), 135.
(68) Edler, K. J.; Reynolds, P. A.; White, J. W.; Cookson, D. *J. Chem. Soc. Faraday Trans.* **1997**, *93* (1), 199.
(69) Flodstrom, K.; Teixeira, C. V.; Amenitsch, H.; Alfredsson, V.; Linden, M. *Langmuir* **2004**, *20* (12), 4885.
(70) Pitcher, M. W.; Ushakov, S. V.; Navrotsky, A.; Woodfield, B. F.; Li, G. S.; Boerio-Goates, J.; Tissue, B. M. *J. Am. Ceram. Soc.* **2005**, *88* (1), 160.
(71) Li, Q. H.; Navrotsky, A.; Rey, F.; Corma, A. *Microporous Mesoporous Mater.* **2003**, *59* (2−3), 177.

Table 3. Measured and Calculated Calorimetric Data

sample	$\Delta H_{dropsol}$ (J/mg)	no. of data points	error (J/mg)	$\Delta H_{dropsol}$, uncorrected (kJ/mol SiO_2)	error (kJ/mol SiO_2)	water correction (kJ/mol)	$\Delta H_{dropsol}$, corrected (kJ/mol)	ΔH_{form}^{298} (kJ/mol)
quartz	0.665	10	0.013	39.97	0.78	0.64	39.97	0.00
MCM-41_1	0.402	14	0.016	20.64	0.98	3.93	20.64	19.33
MCM-41_2	0.407	8	0.008	21.01	0.49	3.86	21.01	18.96
SBA-15_1	0.326	12	0.009	16.77	0.56	3.08	16.77	23.20
SBA-15_2	0.328	10	0.007	16.48	0.39	3.53	16.48	23.49
SBA-15_3	0.296	10	0.009	15.25	0.54	2.75	15.25	24.72
SBA-15_4	0.304	12	0.023	15.43	1.38	3.08	15.43	24.54
SBA-15_5	0.298	12	0.027	13.86	0.99	4.38	13.86	26.11
SBA-15_6	0.299	12	0.022	14.21	1.53	4.07	14.21	25.76
SBA-15_7	0.311	16	0.025	14.75	1.29	4.29	14.75	25.22
SBA-15_8	0.299	12	0.014	15.39	0.81	2.79	15.39	24.58
SBA-15_9	0.263	12	0.015	12.85	0.88	3.17	12.85	27.12
SBA-15_10	0.267	12	0.008	13.27	0.48	2.98	13.27	26.70
SBA-15_11	0.251	10	0.008	12.38	0.50	2.89	12.38	27.59
SBA-15_12	0.183	12	0.024	8.58	0.94	2.53	8.58	31.39
SBA-15_13	0.180	10	0.024	8.65	1.53	2.28	8.65	31.32
MCM-48_1	0.312	18	0.010	15.29	0.74	3.76	15.29	24.68
MCM-48_2	0.290	12	0.012	14.91	0.61	2.72	14.91	25.06
SBA-16_1	0.255	12	0.006	13.37	0.37	2.09	13.37	26.60
SBA-16_2	0.284	12	0.019	15.35	1.13	1.85	15.35	24.62

It was mentioned above that the formation enthalpy of zeolites has a strong correlation with framework density or molar volume, as denser frameworks possess more stable structures relative to less dense polymorphs. Here, in the same manner, MS with higher pore volume are less stable. Figure 4a shows the formation enthalpy vs molar volume for the MS studied along with the data for zeolites.[42] The molar volume is calculated by adding the molar pore volume by the KJS method and molar volume of amorphous silica. Our data seem to follow the general trend for zeolites, though significant scatter is observed, possibly due to higher uncertainty in pore volume measurements and unaccounted variations of MS density.

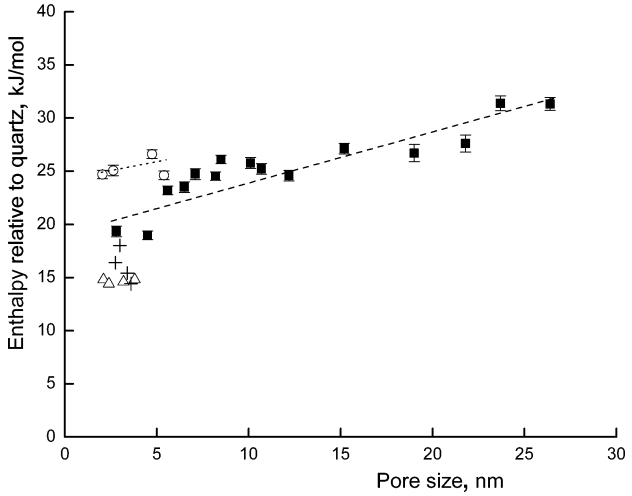

Figure 3. Enthalpies of formation of pure-silica mesoporous materials relative to quartz as a function of pore size: ■, SBA-15 and MCM-41 materials; ○, MCM-48 and SBA-16 materials; △, MCM-41 from refs 21-23; +, MCM-41 materials from ref 72.

A more detailed analysis suggests that the samples studied should be divided into small groups on the basis of framework symmetry and the use of SDA. Figure 5a shows the transition enthalpy as a function of total surface area measured by nitrogen adsorption for all hexagonal MS. The slope of a linear fit yields a surface enthalpy of 0.27 ± 0.15 J/m^2, somewhat higher than the value obtained for silica zeolites and amorphous silica by Moloy et al.[73] The large error due to data scatter indicates that no master plot exists. The use of different SDA and posttreatment under different conditions are likely to result in variations of local framework structure and affect the energetics. As seen from Table 1,

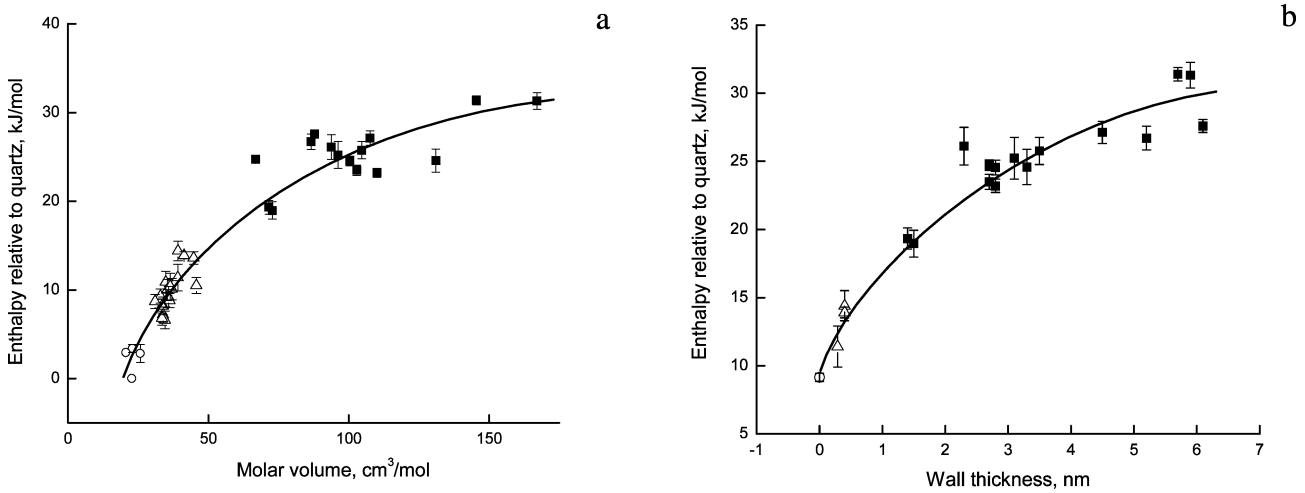

Figure 4. ■ represents enthalpies of formation of pure-silica mesoporous materials relative to quartz as a function of molar volume (a) and wall thickness (b). Data for zeolites (△) and high-density silica polymorphs and amorphous silica (○) are from ref 42. Lines are guides for the eyes.

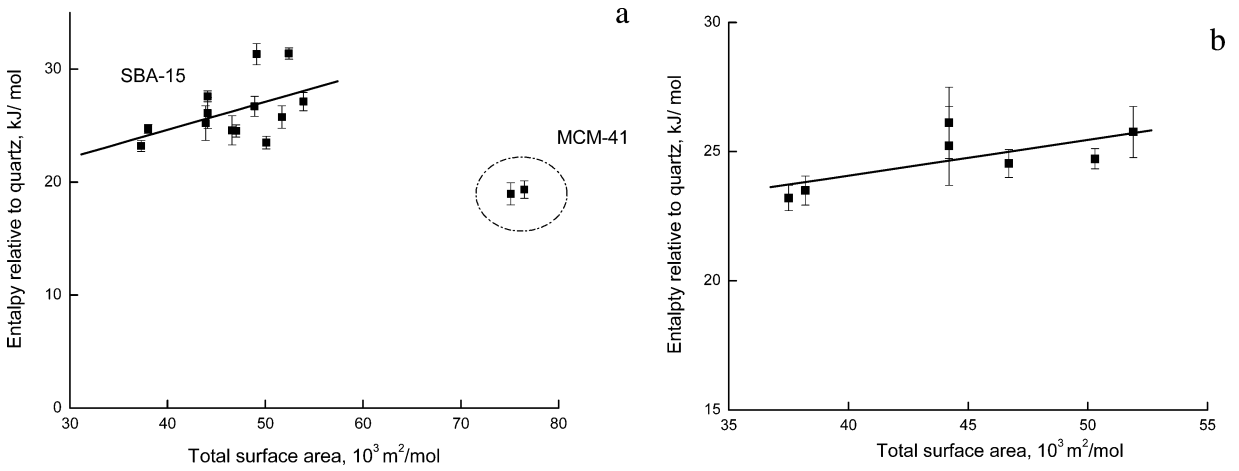

Figure 5. Enthalpies of formation of (a) hexagonal MCM-41 and SBA-15 and (b) SBA-15 (synthesized without TMB) relative to quartz as a function of total surface area.

the structural parameters, such as wall thickness, internal surface area, and internal/external surface area ratio vary significantly and nonmonotonically with pore diameter. Therefore, in addition to the surface enthalpy due to extensive internal surface area, the particle size and surface defect chemistry may also contribute to the formation enthalpy of MS. We did not specifically investigate the morphology of mesoporous silica and particle size effects on energetics. We can refer to TEM studies done by others on similar silicas[74] and our group publication regarding particle size effects in systems with large internal surface area.[75] According to our primary TEM results on selected mesoporous silicas, the typical particle size is in the submicrometer (rather than nanometer) range and should affect the energetics only marginally.

A Transition from Small Pore Hexagonal MCM-41 to Large Pore SBA-15. The measured values for two MCM-41 samples with pore sizes 2.8 and 4.4 nm are 19.3 ± 1.0 and 19.0 ± 0.5 kJ/mol. For MCM-41 with pores from 2.1 to 3.8 nm, the enthalpy relative to quartz was found by Navrotsky et al.[21,22] to be roughly independent of pore size. Our data confirm the pore size independence of energetics for MCM-41 within the available pore sizes. Though slightly higher, our values are in reasonable agreement with the average previous values of 14.6 ± 0.9 kJ/mol obtained using solution calorimetry by Navrotsky et al.[21,22] and 14.4−18 kJ/mol reported by Lee.[72] The slight discrepancy between this work and previous studies by Navrotsky et al.[21,22] may be due to several factors. First, samples used were different. Second, for solution calorimetry, the sample is kept overnight at 973 K and may anneal out some defects, making it more stable. Third, the heat content difference between MCM-41 and quartz contribute to the difference in enthalpy of transformation at 298 and 973 K, making the latter an estimated 1−2 kJ/mol less endothermic, reflecting the energetics of the $\alpha\angle\beta$ quartz transition.

The effect of pore size increase on energetics becomes more pronounced with larger pores. As the pore size increases from 5.6 to 26.4 nm for hexagonal MS, the enthalpy relative to quartz becomes more endothermic, changing from 23.2 ± 0.6 to 31.4 ± 1.4 kJ/mol.

It is safe to conclude that present and previous studies[21,22] show that MCM-41 silica is destabilized by 15−19 kJ/mol relative to quartz, and only by 1−5 kJ/mol compared to siliceous zeolite Y with the most open pore structure (0.74 nm pores). One may speculate that thicker walls (Table 1) stabilize structurally the 2-fold increase in pore diameter for MCM-41. In accord with previous data, our combined SAXS, XRD, and nitrogen adsorption data suggest that MCM-41 materials are characterized by relatively smooth walls and absence of micropores.

We must emphasize that a significant enthalpy difference for hexagonal phases MCM-41 and SBA-15 is observed. This difference can be attributed to differences in the wall microstructure for two classes of MS. SBA-15 materials are synthesized with a block copolymer as SDA instead of CTAB used for MCM-41. In addition, the silica chemistry is completely different: MCM-41 and SBA-15 materials are made under basic and acidic conditions, respectively. The Pluronics copolymer is reported to penetrate into the silica walls, leading to an extended silica precursor−block copolymer interface for SBA-15.[76,77] Upon calcination, the removal of the SDA results in structurally defective and rough channel surfaces and formation of micropores (interchannels), which connect structured mesopores in SBA-15. Our SAXS analysis yields similar scaling parameters in the range of 2.05−2.15 for MCM-41 and SBA-15. This implies that the surface structure for both MCM-41 and SBA-15, with some roughness observed, is almost identical at the nanoscale >1 nm, so the differences may show up only on a smaller scale. A significant micropore volume as measured by nitrogen adsorption for SBA-15 samples (see Table 1) is an indirect indication of micropores with widths smaller than

(72) Lee, B. MS, UC Davis, Davis, CA, 2003.
(73) Moloy, E. C.; Davila, L. P.; Shackelford, J. F.; Navrotsky, A. *Microporous Mesoporous Mater.* **2002**, *54* (1−2), 1.
(74) Zhao, D. Y.; Sun, J. Y.; Li, Q. Z.; Stucky, G. D. *Chem. Mater.* **2000**, *12* (2), 275.
(75) Li, Q. H.; Yang, S. Y.; Navrotsky, A. *Microporous Mesoporous Mater.* **2003**, *65* (2−3), 137.
(76) Goltner, C. G.; Smarsly, B.; Berton, B.; Antonietti, M. *Chem. Mater.* **2001**, *13* (5), 1617.
(77) Smarsly, B.; Goltner, C.; Antonietti, M.; Ruland, W.; Hoinkis, E. *J Phys. Chem. B* **2001**, *105* (4), 831.

2 nm, directly proven by Kruk et al.[62] using the replica method.

One can estimate the surface area of micropores that corresponds to the 4 kJ/mol difference between MCM-41 and SBA-15 within the 4−6 nm pore size range. A simple calculation based on surface enthalpy for SBA-15 (0.13 ± 0.04 J/m^2) yields 390−740 m^2/g. This value contradicts the surface area of 60−80 m^2/g, estimated from the micropore to mesopore volume ratio (Table 1) and the total surface area. These calculations imply that it is impossible at this stage to calculate the energy contribution due to micropores and assign the enthalpy difference between hexagonal MCM-41 and SBA-15 solely to micropores.

A silica source and acidic or basic synthesis conditions may also affect the energetics of MS. Petrovic et al.[21,22] studied MCM-41 samples synthesized under acidic and basic conditions and did not find differences in enthalpies. In this study we used two silica sources for MCM-41 synthesis (see Experimental Section) and found no significant change in enthalpies relative to quartz. We realize that silica chemistry itself is an important factor in controlling microstructure of MS walls. On the other hand, the use of a different SDA has a direct effect on the chemistry of the silica wall surface during synthesis and calcination steps. Therefore, to investigate whether energetics of MS is indeed influenced by acidic and alkaline media, one would have to make SBA-15 materials with a wide span of pore sizes under basic conditions. This has not been possible so far.

Another interesting finding is that the energetics of hexagonal MS correlates with wall thickness (see Figure 4b). For comparison, calorimetric results for selected zeolites with most open structures and channels significantly larger than the tetrahedron size[42] along with silica glass are shown in Figure 4b. Other zeolites studied have either complex frameworks, where the term "wall" is hard to define, or small channels whose sizes are close to the tetrahedron size and small (three-, four-, five-, and six-membered rings). The "wall thickness" for zeolites is estimated as a difference between the cell size for the corresponding basal plane and channel diameter.[78] The size of large (eight- and 12-membered) rings is used as an estimate of the pore size rather than standardized pore sizes for zeolites because it is closer to the definition of "effective" wall thickness of MS. Bulk amorphous silica has no pores and, therefore, no walls. In other words, for comparison purposes, bulk silica may be considered to be "porous" with pores whose sizes are indistinguishable from the tetrahedron size within the error of pore size determination for MS (0.1−0.2 nm).

In contrast to all other samples, SBA-15 materials, synthesized without TMB, represent a self-consistent class of MS with a wide range of pore sizes characterized by monotonic variations in external and internal surface areas. Therefore, SBA-15 provides a unique opportunity to analyze the energetics−surface area relationship and estimate the surface enthalpy. The enthalpy relative to quartz as a function of total surface area measured by nitrogen adsorption is plotted for SBA-15 without TMB (Figure 5b). The data points for seven samples without TMB lie on a single linear plot with a slope of 0.13 ± 0.04 J/m^2, which is in agreement with the surface enthalpy of 0.10 ± 0.035 J/m^2 based on previous calorimetric results and computer simulations for silica polymorphs and zeolites. The data were error-weighted in the fit. The slope for nonweighted data changes insignificantly from 0.13 ± 0.04 to 0.14 ± 0.05 J/m^2. Thus for the first time, the surface enthalpy for MS is estimated on the basis of direct calorimetric results.

Cubic MCM-48 and SBA-16. As the pore size increases from 2.1 to 5.4 nm for cubic MS, the enthalpy relative to quartz changes marginally from 24.6 to 26.6 kJ/mol. This is 5−7 kJ/mol above MCM-41 in the same range of pore sizes, indicating that the cubic phase is less stable than the hexagonal one.

The Role of Framework Structure in Energetics of MS. In contrast to well-ordered zeolites, mesoporous silicas represent a class of materials in which hollow channels are arranged in crystalline-like structures, whole walls are essentially amorphous.[1,5] The enthalpy of mesoporous MCM-41 silica materials relative to silica glass is 6−10 kJ/mol. Petrovic et al. attributed this value to higher concentration of strained three-membered and four-membered siloxane rings in MCM-41 compared to that in fused silica.

Silica glass is described by a continuous network of a distribution of rings consisting of Si atoms in corner-shared SiO_4 tetrahedra with bridging oxygens linked to two adjacent silicons. The six-membered rings are reported to be dominant.[79−81] The network of pure silica is disrupted by defects made of geminal SiO_2−(OH) and single SiO_3−(OH) silanols (Q^2 and Q^3 sites in NMR terminology). The two-, three-, and four-membered rings are strained and form as a result of condensation of silanols into siloxane bridges upon dehydroxylation on the silica surface. The four-membered rings are only weakly strained compared to rings in α-quartz. The highly strained two- and three-membered rings are metastable with respect to silanol groups, as evidenced by their high reactivity with water.[82] A very low concentration of two-membered rings was previously detected by infrared spectroscopy[83,84] at 888 and 908 cm^{-1}. The evidence for three- and four-membered rings in silica glass was provided by Raman and ^{29}S MAS NMR spectroscopy,[64,65] and supported by ab initio simulations.[79−81,85,86]

There is a huge body of Raman spectroscopic data dedicated to MS and MS supported catalytic materials.[28−31,33,34,87−92]

(78) Fenelonov, V. B.; Derevyankin, A. Y.; Kirik, S. D.; Solovyov, L. A.; Shmakov, A. N.; Bonardet, J. L.; Gedeon, A.; Romannikov, V. N. *Microporous Mesoporous Mater.* **2001**, *44*, 33.
(79) Rino, J. P.; Ebbsjo, I.; Kalia, R. K.; Nakano, A.; Vashishta, P. *Phys. Rev. B* **1993**, *47* (6), 3053.
(80) Dellavalle, R. G.; Andersen, H. C. *J. Chem. Phys.* **1992**, *97* (4), 2682.
(81) Vollmayr, K.; Kob, W.; Binder, K. *Phys. Rev. B* **1996**, *54* (22), 15808.
(82) Du, M. H.; Kolchin, A.; Cheng, H. P. *J. Chem. Phys.* **2004**, *120* (2), 1044.
(83) Bunker, B. C.; Haaland, D. M.; Michalske, T. A.; Smith, W. L. *Surf. Sci.* **1989**, *222* (1), 95.
(84) Bunker, B. C.; Haaland, D. M.; Ward, K. J.; Michalske, T. A.; Smith, W. L.; Binkley, J. S.; Melius, C. F.; Balfe, C. A. *Surf. Sci.* **1989**, *210* (3), 406.
(85) Uchino, T.; Tokuda, Y.; Yoko, T. *Phys. Rev. B* **1998**, *58* (9), 5322.
(86) Donadio, D.; Bernasconi, M., 2004.
(87) Geidel, E.; Lechert, H.; Dobler, J.; Jobic, H.; Calzaferri, G.; Bauer, F. *Microporous Mesoporous Mater.* **2003**, *65* (1), 31.
(88) Xiong, G.; Li, C.; Li, H. Y.; Xin, Q.; Feng, Z. C. *Chem. Commun.* **2000** (8), 677.

Due to the inherent sensitivity of Raman bands to extensive specific surface area, a comparative analysis of concentration of three- and four-membered ring is not possible. Moreover, the relative intensity of a band due to silanol groups (at 980 cm^{-1}) is believed to correlate with the formation of three-membered rings upon dehydroxylation of the silica surface[93] and, therefore, strongly depends on thermal history, which, in turn, hampers the comparison of our results with the literature data. Nevertheless, some qualitative conclusions can be drawn.

Raman results by Brinker et al.[64] showed bands at 490 and 608 cm^{-1} associated with three- and four-membered siloxane rings in amorphous silicas. Similarly, bands at 490−492 and 605−610 cm^{-1} were assigned to three- and four-membered rings in MCM-41.[87,88] According to recent studies by Raman spectroscopy,[33,88] SBA-15 has features similar to MCM-41, namely bands at 485 and 603 cm^{-1}, corresponding to siloxane rings. A strong Raman band at about 980 cm^{-1}, related to silanol groups, was found in all MCM and SBA samples.[33,87,88] In comparison with fumed silica, the silanol band intensity is low, but three- and four-membered ring bands have relatively higher intensity for MCM-41, which can be either due to a higher fraction of these structural units in the MS or just larger surface area.

^{29}Si MAS NMR spectroscopy is a powerful tool to provide quantitative information on the concentration of hydroxyl defects in silica. ^{29}Si MAS NMR spectra of silica show peaks corresponding to silicon atoms in $Si(OSi)_2(OH)_2$ (Q^2 peak), $Si(OSi)_3(OH)$ (Q^3), and $Si(OSi)_4$ (Q^4) environments. The spectra are dominated by a Q^4 peak with a maximum between −110 and −111 ppm. This maximum is related to the average Si−O−Si angle of 148−150°, obtained using a relationship by Oestrike et al.[94] Brinker et al.[64] first deconvoluted the amorphous silica ^{29}Si NMR spectra to account for three-membered rings. Their simple model is based on the assumption that Q^4 of three-membered rings appears at about −105 ppm due to a smaller Si−O−Si angle of 139°. To the best of our knowledge, there has been no attempt to analyze ^{29}Si NMR spectra data in terms of the three-membered rings for MS. The difficulty in detection of three-membered rings results from the relatively low concentration of the Q^2 and Q^3 as well as low resolution of the Q^n sites for calcined MS. In addition, some assumptions regarding positions and breadths of the peaks have to be made. In agreement with previous studies of amorphous and mesoporous silica, ^{29}Si CP MAS NMR spectra show well-resolved Q^2 and Q^3 peaks at about −92 and −101 ppm (Figure 2d), so their chemical shifts can be kept fixed in ^{29}Si MAS NMR spectrum deconvolution.

Table 4. Results of ^{29}Si MAS NMR Spectrum Deconvolution for Selected Samples

sample	$Q^2 + Q^3$ (%)	$Q^2 + {}^1/_2Q^3$ (%)	Q^4 (%)
MCM-41_1	10	5.6	20
MCM-48_2	10	5.3	25
SBA-15_4	10	5.3	24
SBA-15_5	15	6	27
SBA-15_6	13.5	7.8	30
SBA-15_7	7.8	4	24
SBA-15_12	7.8	4.2	33
SBA-15_13	6.8	3.7	28

Our attempts to deconvolute ^{29}Si MAS NMR spectra into only three peaks, belonging to Q^2, Q^3, and Q^4, result in either unusual chemical shifts for Q^2 and Q^3 defects, when peaks are allowed to float, or abnormally high concentrations for them, when peaks are fixed. In all scenarios a peak between −103 and −106 ppm is required to arrive at a statistically reasonable deconvolution (Figure 2). The use of our deconvolution method (for details see Experimental Section) led to -105 ± 1 ppm for the $Q^{4'}$ chemical shift. Previous studies by Sen et al.[95] and Gladden et al.[96] showed the exceptional usefulness of this approach for the analysis of silicate glasses. The deconvolution results (Table 4) are in good agreement with our TG data and concentrations of Q^2 and Q^3 defects of calcined SBA-15 obtained by a direct method utilizing ultrafast spinning ^{1}H NMR spectroscopy.[26] To compare our results with an earlier study,[26] one has to calculate $Q^2 + Q^3$ instead of $Q^2 + Q^3/2$. The former yields 0.07−0.15 for our SBA-15 samples compared to 0.15 obtained in that study; 20−32% of the defects are due to strained rings, which seems high but is in accord with previous studies on silica gels.[64,65,96]

Sen et al.[95] studied K_2O-SiO_2 with high silica content by ^{29}Si and ^{17}O NMR spectroscopy. They argue that a peak at −105 ppm corresponds to Q^4 sites, directly linked to Q^2 and Q^3 sites, as evidenced by a linear dependence of the integral under the $Q^{4'}$ peak as a fraction of Q^2 and Q^3. At first sight these results are in contradiction to NMR and neutron diffraction studies of silica gels dehydrated at various temperatures, in which fractions of Q^2 and Q^3 decrease with increasing intensity of the $Q^{4'}$ peak and vice versa.[96] Both points of view can be reconciled if one assumes that a significant fraction of $Q^{4'}$ sites shares three-membered rings with Q^2 or/and Q^3 sites to accommodate the highly strained configurations. For these reasons, the concentration of the strained rings might be overestimated. However, our enthalpies of MS correlate well with the obtained concentrations of strained rings and, at present, it is not possible to distinguish contributions from Q^4's which are part of strained rings and next to Q^2 and Q^3 sites. Nevertheless, TGA and ^{29}Si NMR results together support our interpretation of the $Q^{4'}$ peak that the concentration of hydroxyls is 2−3 times lower than the corresponding $Q^{4'}$ intensity observed in calcined samples.

Interestingly, the calculated concentration of $Q^{4'}$ sites is almost 1.5 times higher for less stable SBA-15 (24−32%) compared to that for more stable MCM-41 (20%). Therefore,

(89) Fornes, V.; Lopez, C.; Lopez, H. H.; Martinez, A. *Appl. Catal. A Gen.* **2003**, *249* (2), 345.
(90) Hess, C.; Hoefelmeyer, J. D.; Tilley, T. D. *J. Phys. Chem. B* **2004**, *108* (28), 9703.
(91) Liu, Y. M.; Cao, Y.; Yi, N.; Feng, W. L.; Dai, W. L.; Yan, S. R.; He, H. Y.; Fan, K. N. *J. Catal.* **2004**, *224* (2), 417.
(92) Segura, Y.; Cool, P.; Van Der Voort, P.; Mees, F.; Meynen, V.; Vansant, E. F. *J. Phys. Chem. B* **2004**, *108* (12), 3794.
(93) Kinowski, C.; Bouazaoui, M.; Bechara, R.; Hench, L. L.; Nedelec, J. M.; Turrell, S. *J. Non-Cryst. Solids* **2001**, *291* (3), 143.
(94) Oestrike, R.; Yang, W. H.; Kirkpatrick, R. J.; Hervig, R. L.; Navrotsky, A.; Montez, B. *Geochim. Cosmochim. Acta* **1987**, *51* (8), 2199.
(95) Sen, S.; Youngman, R. E. *J. Non-Cryst. Solids* **2003**, *331* (1−3), 100.
(96) Gladden, L. F.; Vignaux, M.; Chiaranussati, P.; Griffiths, R. W.; Jackson, S. D.; Jones, J. R.; Sharratt, A. P.; Robertson, F. J.; Webb, G.; Chieux, P.; Hannon, A. C. *J. Non-Cryst. Solids* **1992**, *139* (1), 47.

both our NMR data and the Raman results by others show that the number of strained rings and extensive internal surface (high molar volume) are the key factors in placing silica polymorphs on the energy landscape. At present it is not possible to separate defects representing strained rings in the bulk, which relate to the component of the formation enthalpy independent of surface area and defects on the surface, which contribute to the surface enthalpy. It might not even be possible to separate bulk and surface effects, since the walls are only 1−6 nm thick. On the other hand, since surface hydroxyls are believed to be precursors of the strained rings, one can assume that such rings form predominantly close to the surface.

In this regard, the fact that less stable hexagonal MS have thicker walls (see Figure 4b) deserves particular attention. Much of the ring strain probably develops during the calcination process, in which the silica framework condenses and shrinks. At that point the high-energy bonding configurations are formed and kinetically locked. Under basic conditions as for MCM-41, the silica is probably much more cross-linked as it assembles. As a result, there is less potential for shrinkage upon calcination and less formation of strained rings, This is in agreement with our and other studies in which larger unit cell contractions are observed for SBA-15 materials. For example, Kleitz et al.[97] reported larger contraction (13%) of the hexagonal unit cell for SBA-15-type material compared to that of MCM-41 (6−10%). In contrast to this observation, the calcination of aged MCM-41 led to only a 3−5% contraction, which is in agreement with our lattice contraction measurements. The contractions for some SBA-15 in the Zhao et al. study[41,98] are even smaller (1−3%). These different results are probably due to aging in mother liquor used as an intermediate step in the preparation process. The enthalpy relative to quartz (at constant pore size) increases as the walls become thicker, because the number of strained rings increases. Another possible scenario is that, if the strained rings are formed on the surface, thicker walls are probably needed to stabilize the framework and compensate the increasing number of strained rings on surface of MS with larger pores.

Another important finding of this study is that the cubic phase is less stable than the hexagonal within the same range of pore sizes. This result is in agreement with previous studies of the hexagonal to cubic transition, which is endothermic.[99] Moreover, cubic samples have somewhat higher concentrations (25%) of strained rings compared to MCM-41 (20%).

Therefore, here we can make a very important conclusion concerning the energetics of MS: the concentration of ring defects correlates with the formation enthalpy of MS.

This work attempted to answer one of the fundamental questions relevant to formation of porous silica-based materials: how pore size, framework density, and symmetry of the silica channel structure affect the thermodynamic stability of the framework. This study confirms that MS, not only zeolites as established before, follow the general trend: less dense frameworks occur at the expense of higher instability. However, a more detailed picture of the structure−energy relationship for calcined MS frameworks has emerged. We emphasize here that the MS framework must be viewed as being formed during two stages: (1) mesoscopic self-assembly of the inorganic precursor and SDA, followed by framework condensation, and (2) structural rearrangement due to dehydroxylation and postcondensation during aging and calcination. At each stage the driving forces for framework assembly, influencing enegetics and structure, are different.

It was predicted a decade ago by Navrotsky et al.,[21,22] and is still supported by the newer data, that the energy differences between various calcined frameworks are small and on the order of thermal energy. Thus, at initial stages the framework self-assembly is governed by small differences in energy between competing strongly and weakly bonded species in a multicomponent system of water, silica precursor, and SDA. These small differences are the key to why so many different structures can form. At final stages of thermal posttreatment, the framework undergoes structural rearrangements that involve dehydroxylation and postcondensation. The condensation of hydroxyls into siloxane rings is affected geometrically by accessibility of OH groups to each other, kinetically by temperature and time and thermodynamically by the equilibrium of silanols with water in confined geometry (in micro and mesopores). At initial stages the use of different SDA determines the microstructure of channels, whereas at final stages the framework is prone to changes in concentration of hydroxyl groups and strained rings in a complex way, depending on the above-mentioned geometrical, kinetic, and thermodynamic factors.

Conclusions

Hexagonal (MCM-41, SBA-15) and cubic (MCM-48, SBA-16) mesoporous silicas have been synthesized and their energetics characterized by high-temperature drop solution calorimetry using lead borate solvent at 974 K. The use of a wide range of pore sizes, 2.1−26.4 nm, allowed us to elucidate effects of pore size and molar volume on energetics. On a large energy scale, the formation enthalpy is found to be linearly dependent on pore size in a range of energies from 19 to 31 kJ/mol relative to quartz (from 10 to 21 kJ/mol relative to dense amorphous phase). This quite narrow range imposes little energetic limitations to synthesis of mesoporous structures, which can be overcome by the thermal energy and/or competitive contributions due to interactions among silica, water, and structure-directing agent. On a small energy scale, the concentration of hydroxyl groups and strained rings plays an important role in energetics of mesoporous silicas. SBA-15 has more ring defects and micropores compared to MCM-41. Within the 4−6 nm pore size range, hexagonal SBA-15 and cubic SBA-16 silicas are similar in terms of energetics and ring defects. Interestingly, despite different origins, the cubic MCM-48 and SBA-16 samples have similar formation enthalpies and are less stable

(97) Kleitz, F.; Schmidt, W.; Schuth, F. *Microporous Mesoporous Mater.* **2003**, *65* (1), 1.
(98) Yang, P. D.; Zhao, D. Y.; Margolese, D. I.; Chmelka, B. F.; Stucky, G. D. *Nature* **1998**, *396* (6707), 152.
(99) Landry, C. C.; Tolbert, S. H.; Gallis, K. W.; Monnier, A.; Stucky, G. D.; Norby, F.; Hanson, J. C. *Chem. Mater.* **2001**, *13* (5), 1600.

than MCM-41 within the 2−5 nm pore size range, possibly due to a higher concentration of strained rings.

Acknowledgment. This research was supported by the National Science Foundation (NSF) grant DMR 01-01391. S.H.T. is an Alfred P. Sloan Foundation Research Fellow. Prof. Sabyasachi Sen is acknowledged for fruitful discussion of NMR results. The authors thank Dr. Eric Moloy, for his computer calculations of mesoporoues silica and discussions, and Dr. Ping Yu, for assistance with NMR experiments. The authors also acknowledge Dr. Sergey Ushakov, for TEM analysis on selected MS samples, and the National Center for Electron Microscopy at the Lawrence Berkeley National Laboratory, for the use of its facilities.

CM050366G